PROCEEDINGS OF SCIENCE

ICRC 2021
THE ASTROPARTICLE PHYSICS CONFERENCE
Berlin | Germany
37th International Cosmic Ray Conference
12–23 July 2021

Optimization of CoREAS simulations for the GRAND project

Chao Zhang,[a,b,c,*] **Tim Huege**[a,d] **and Tanguy Pierog**[a] **on behalf of the GRAND Collaboration**
(a complete list of authors can be found at the end of the proceedings)

[a] *Institute for Astroparticle Physics (IAP), Karlsruhe Institute of Technology, Karlsruhe, Germany*
[b] *Kavli institute for astronomy and astrophysics, Peking University, Beijing, China*
[c] *Department of Astronomy, School of Physics, Peking University, Beijing, China*
[d] *Astrophysical Institute, Vrije Universiteit Brussel, Brussels, Belgium*

E-mail: chao.zhang@kit.edu

A planned array of 200,000 antennas covering an area of 200,000 km ^{2} – the GRAND project – is proposed to detect cosmic-ray, gamma-ray, and neutrino primaries in the energy range beyond 10^{17}eV. The GRAND array will be able to detect upward-going air showers initiated by neutrino interactions in the rocks on its mountainous site, furthermore, it may also detect very inclined and atmosphere-skimming air showers initiated by cosmic rays. So the corresponding shower geometry differs from the other experiments and asks for a detailed investigation. To meet the requirements of GRAND, we develop an update of CORSIKA7 for the simulation of upward-going air showers. Furthermore, we apply today's best knowledge of parameters of the GRAND project, in particular realistic on-site atmospheres, in an extensive library of inclined air showers. Finally, we evaluate expected signal-to-noise ratios and detection thresholds for the GrandProto300 (GP300) phase of GRAND.

37th International Cosmic Ray Conference (ICRC 2021)
July 12th – 23rd, 2021
Online – Berlin, Germany

*Presenter

PoS(ICRC2021)248

1. Introduction

The geomagnetic effect and Askaryan effect contribute together to produce radio emission during the development of air showers created by a neutrino, a charged particle or a gamma ray. The radio emission can be received by antennas deployed above the ground, and the related techniques of radio detection of air showers have developed rapidly in the last 2 decades [1].

Downward-going air showers induced by ultra high energy cosmic rays (UHECRs) have been detected in several experiments. Different from the previous detection strategy, GRAND has planned much larger antenna layouts which will increase its exposure to an unprecedented level [2], and it will extend the radio detection to zenith angles larger than 90°. The interactions between an UHE τ neutrino with the high-density material in the mountains create high energy τ particles. These have a relatively larger mass than μ and e^- and traverse a long distance in the rock and then can exit into atmosphere to decay in the vicinity of the antennas. Previously, upward-going air showers with a zenith angle above 90° have only been reported in the ANITA experiment [3]. Yet it will be the dominant detection channel of neutrinos in GRAND, which is the main difference from other experiments. For UHE primary particles coming from horizontal directions, the radio-emission footprint initiated by air showers can reach up to 100 km^2 on the ground [4], so horizontal atmospheric showers are also expected. The predicted UHECR event rate will be 20 times larger than that of the Pierre Auger Observatory when the GRAND array is fully deployed [2].

CoREAS is a Monte Carlo tool to simulate radio emission of extensive air showers using the "endpoint formalism" to take into account emission created by acceleration of charged particles [5, 6]. It has been successfully applied in previous radio detection experiments such as KASCADE [7], LOPES [8] and LOFAR [9], AERA [10] and others. CoREAS needs a model of the refractive index of the atmosphere to properly describe Cherenkov effects. Thus an investigation of a representative atmosphere for the GP300 site is done in this work (see section 2). CoREAS is implemented in CORSIKA [11] to use the information of each tracked particle (position, time). But in the existing versions of CORSIKA, there was no working option to simulate upward-going air showers. So the

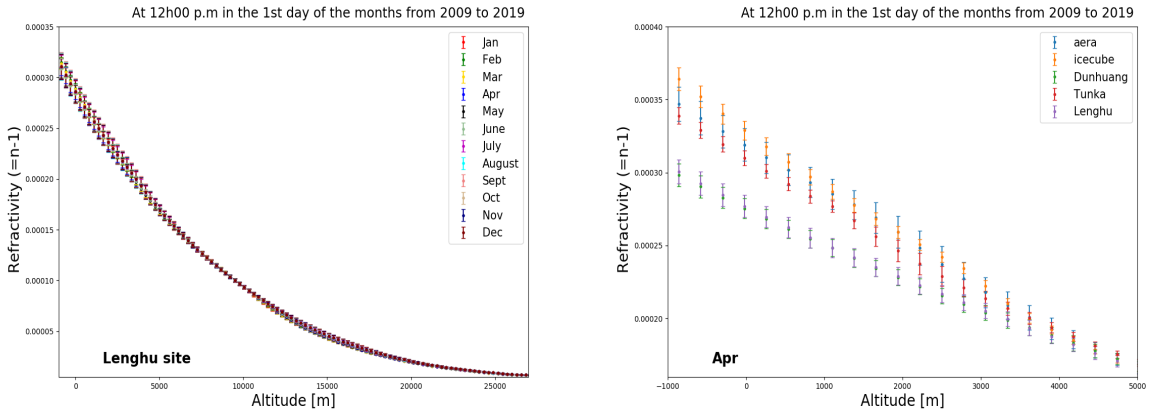

Figure 1: Comparison of the atmospheric conditions for the radio sites from 2009 to 2019. Left: Comparison of averaged atmospheric profiles of each month at the Lenghu site. Right: Comparison with other radio detection sites.

air shower library prepared in this work consists of only downward-going air showers until now. Incorporating detailed information on the GP300 site such as the representative atmospheric model, the geomagnetic field strength and the altitude, we have prepared a library of simulations for air showers with different primary particles, primary energies, zenith and azimuth angles (see section 3). To simulate upward-going air showers, CORSIKA has been updated to enable simulations of air showers with zenith angle $\theta > 90°$. We have used several testing methods to check the internal consistency of this new update (see section 4). The radio detection of air showers works well in the energy range down to several 10 PeV. The LHAASO experiment has reported recently a discovery of gamma ray event at 1.4 PeV [12]. There is an energy gap between the two energy levels. To bridge them, it is useful to study the possibility to detect gamma rays or cosmic rays in the energy range down to 10 PeV in any phase of GRAND. A preliminary SNR analysis demonstrates that it is quite difficult to achieve this goal in GP300 (see section 5).

2. Investigation of representative atmosphere for GP300 site

The depth of the maximum of the air shower evolution, X_{max}, can be measured by radio experiments and is an option to study the primary particle mass composition. The accuracy of the radio-measured Xmax depends on the atmospheric condition since the interactions of cosmic rays with atmospheric nuclei and decays of the secondary particles in the air govern the development of air showers [1]. Until now, there was no detailed study of the atmospheric conditions such as humidity, pressure, temperature, and the index of refraction at the GP300 site, which is a source of systematic uncertainties in the reconstruction [13]. The Global Data Assimilation System (GDAS) is a reliable global atmospheric model which has been applied in Auger and LOFAR [14, 15]. The advantage of the GDAS model is that it provides time-dependent, realistic atmospheric profiles of the location of the experiment.

In this work, the atmospheric data of the GP300 site in Lenghu (38°52'12.0"N, 92°19'48.0"E), China from 2009 to 2019 is collected and analyzed with the GDAS tool implemented in CORSIKA. For each month at the GP300 site, the moment of 12h00 and 0h00 of the 1st day and the 15th day are analyzed with the gdastool to extract the atmospheric parameters, including refractive indices at different altitudes. We compare all the months of each year, and certain days in each year, and then average conditions of each year to select a representative model suitable for air-shower simulations for GRAND.

As shown in Fig. 1 (left), the refractivity at 12h00 PM in the first day of each month from 2009 to 2019 is very similar. So the atmospheric conditions at this site are very stable and in that sense ideal for radio detection. Refractivity decreases slowly from 0.0003 at sea level to below 0.00005 at 25,000 meters wrt sea level. The GP300 site is located at around 2900 m altitude, so the refractive index at ground is $\sim$ 1.00022. In this work, the profile of 1st of June 2012 is chosen as the representative model for all simulations.

A comparison with other radio detection sites such as AERA, IceCube, and Tunka is also made. In addition, another potential GRAND site in Dunhuang near Lenghu is also analyzed. As shown in Fig. 1 (right), the refractivity at the GP300 sites is relatively smaller than that of the other sites, which is not expected. The comparison in the other months leads to the same conclusion.

When there are no extreme weather conditions at the GP300 site, the GDAS profile should be trusted. The simulations in this work are based on it.

3. Preparation of a CoREAS library

To demonstrate the viability of the detection principle of GRAND, the 1st phase GP300 will contain 300 antennas and work in the energy range down to $10^{16.5}$ eV. Then the array will be extended to 10 k and later to 200 k antennas in the next phases and the aimed energy will reach beyond 10^{20} eV [2]. The library is designed to cover the energy range from [10^{16},10^{20}] eV to serve all the phases.

For UHECR, the thinning method needs to be introduced to reduce the computing time by tracking only a fraction of particles. Especially when CoREAS is activated for radio emission simulation, the computing time increases, in particular at large zenith angles. If the thinning level is not small enough, obvious fluctuations in longitudinal distributions are obtained. If the thinning level is too small, large computing resources are required. To balance the computing time and precision, in this library, the thinning level is set as 10^{-6} with optimized maximum weights. The computing time increases up to about 1000 hours for each UHE proton and iron air shower with a zenith angle $\theta = 87°$. All the computations were done on the bwUniCluster 2.0 in Baden-Württemberg. The PARALLEL option in CORSIKA is activated and the jobs are distributed on 5 nodes (64-bit Intel Xeon) with 20 tasks on each of them.

GRAND will be efficient to detect cosmic rays in the zenith-angle range above 65°. For downward-going air showers, CORSIKA 7.7400 is applied with the combination of QGSJetII-04 and URQMD hadronic interaction models and CURVED atmosphere. Until now, simulations of zenith angles from 65° to 87° have been finished. For upward-going air showers above 90°, an updated version of CORSIKA7 has been developed and been tested, a detailed description of this adaptation is given in the next section. Showers at eight azimuth angles { −180°, −135°,−90°,−45°,0°,45°,90°, 135° } are simulated for each zenith angle. The representative atmospheric model at the GP300 site is stored and selected in these simulations. The geomagnetic vector in this work is {B_x,B_z}={26.928,42.154} μT. A star-shaped layout with 240 antennas is configured to receive radio signals. The corresponding response on each antenna generated with CoREAS is stored and processed for further study.

4. Adaptation of CORSIKA7 for upward-going showers and its validation

Two upward-going, shower-like event have been reported by the balloon-based ANITA experiment [3, 16]. But their nature is still unknown. More upward-going air showers are expected to be detected in GRAND, which may help to find an explanation. The GRAND experiment is expected to detect upward-going air showers generated by tau neutrinos interacting in the rock of the mountainous site. Some simulation work of this kind of air showers has been made so far with ZHAireS [2, 17]. Currently, CORSIKA 7 has been adapted to satisfy the requirements of GRAND. To validate this adaption, testing methods are being developed. Downward-going air showers simulated by CORSIKA have been studied and confirmed by several experiments. Hence they can serve as references to check the simulated upward-going air showers. For the sake of

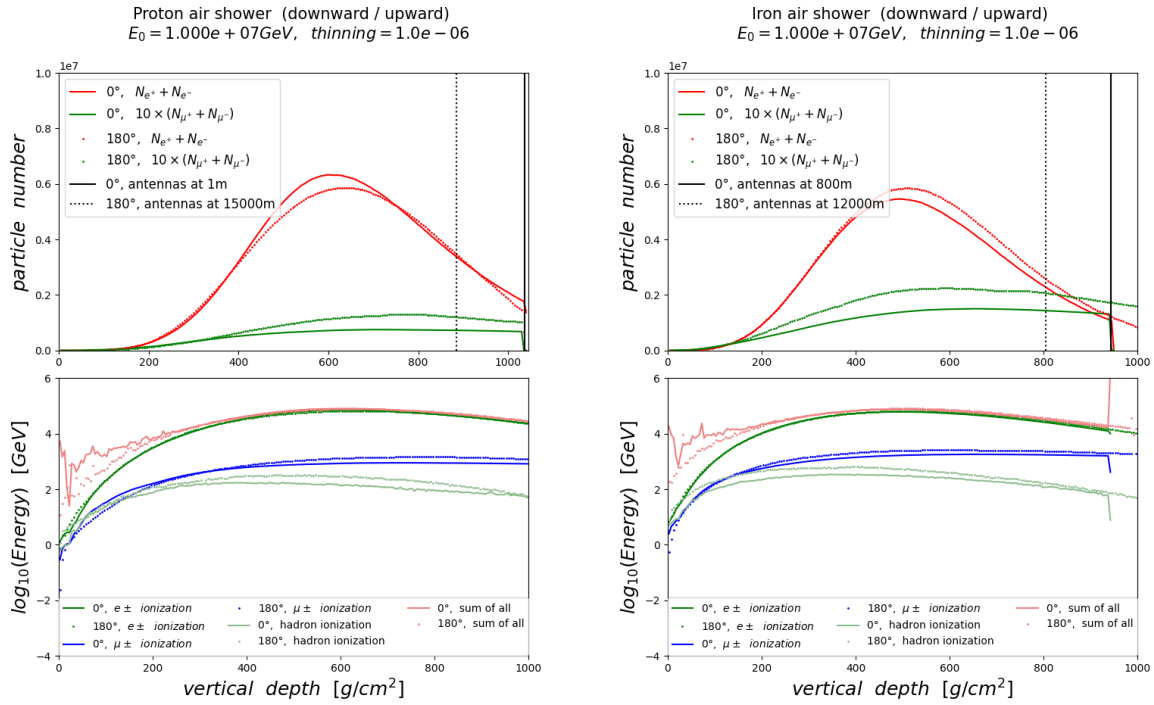

Figure 2: Comparison of the longitudinal distribution of particle number and energy between upward-going air showers (θ = 180°) and downward-going air showers (θ = 0°). Two proton air showers (left) and two iron air shower (right) show their similar longitudinal distributions in upward-going and downward-going directions. The particle numbers are shown on the upper panel, and the energy distributions are shown in the bottom panels. Here the primary energy is 10^{16} eV and thinning level = 10^{-6}.

simplicity, upward-going air showers of zenith angle θ = 180° and downward-going air showers of zenith angle θ = 0° are compared in this work.

The following simulations of proton/Iron air showers were computed to make the comparison in this work:

1. A 10^{16} eV upward-going proton (iron) air shower starting at an observation altitude of 1 m with antennas located at an observation altitude of 15000 m (12000 m), the atmospheric depth of which is illustrated with the dashed line on the left (right) side of Fig. 2.

2. A 10^{16} eV downward-going proton (iron) air shower starting at a random altitude above 8500 m with antennas located at an observation altitude of 1 m (800 m), illustrated with the solid black line at the right edge on the left (right) side of Fig. 2.

For two identical particles originating from opposite directions in the same atmosphere, the propagation of the decay-produced secondary particles could be compared to each other, although the variations of atmospheric density are different. This is shown in the two top panels of Fig. 2, where the particle numbers of e^+ and e^-, μ^+ and μ^- along the vertical depth for the two air showers are very similar for both the proton and iron air showers. For the longitudinal energy deposit, the $e^\pm$ ionization, $\mu^\pm$ and $\mu^\pm$ ionization, the γ energy cut, $\mu^\pm$ energy cut, neutrinos, hadron ionization, hadron energy cut, sum of all are compared, and four of them are shown in the bottom panels. These

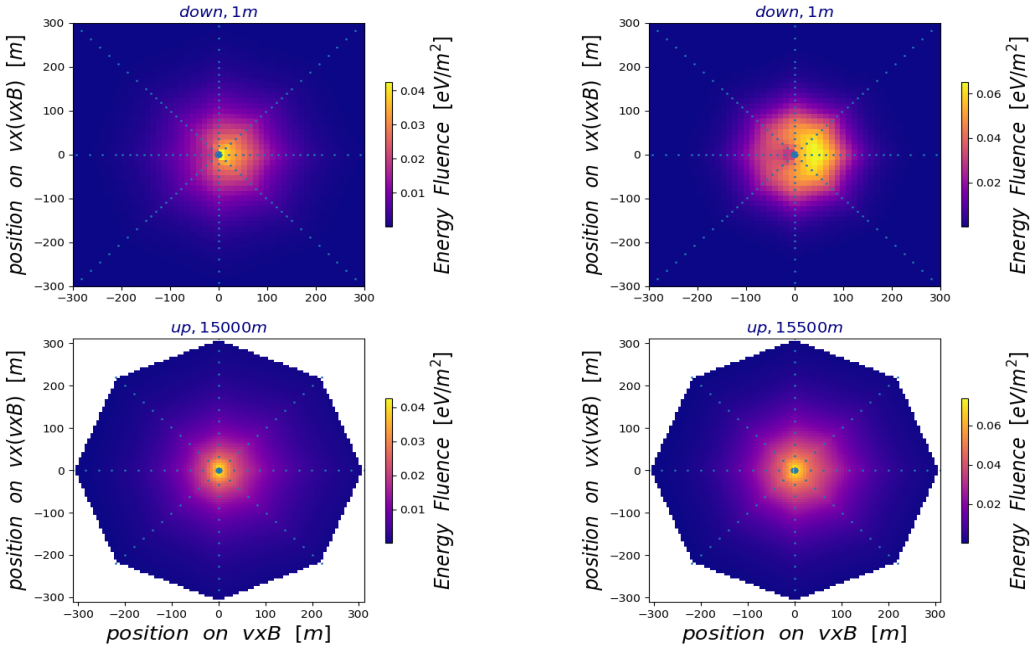

Figure 3: Distribution of the energy fluence in the 30-80 MHz band (left) and the 50-200 MHz band (right) of a downward-going proton air shower with zenith angle $\theta = 0°$ with antennas at an altitude of 1 m a.s.l. (top row) and an upward-going proton air shower with zenith angle $\theta = 180°$ at an antenna altitudes of 15,000 or 15,500 m a.s.l. (lower row).

similarities prove that the particles in the upward-going air showers behave in the same way as the downward-going air showers. If the simulation works correctly, the radiation energy received by the antennas should also agree. Several layers of star-shaped antenna grids were placed at different observation altitudes for the upward-going air showers. The atmospheric depths corresponding to these altitudes are shown with vertical line in Fig. 2 to illustrate that the antennas are located at a roughly comparable stage of the air shower development for both the downgoing and upgoing air showers. Two filters (frequency band 30-80MHz, and 50-200MHz) are applied in this work. This comparison between upward-going and downward-going proton air showers should have similar behaviors of energy deposit if the antenna layouts are placed at proper altitudes. As shown in Fig. 3 , the energy deposits are close but they are not exactly the same since they started in different air densities. For the Iron air shower, the energy deposit leads to the same conclusions.

Another important check is the integral of the energy fluence over the respective radio-emission footprints to determine the total radiation energy received by the antennas. The values are listed in table 1 and show a reasonable agreement between the downgoing and upgoing showers as well as the different altitudes for the antenna grids.

Judging from the particle profile and the agreement between the footprints and radiation energies for the upgoing and downgoing air showers, we conclude that the modifications we made to CORSIKA 7 to enable upward going geometries have been successful.

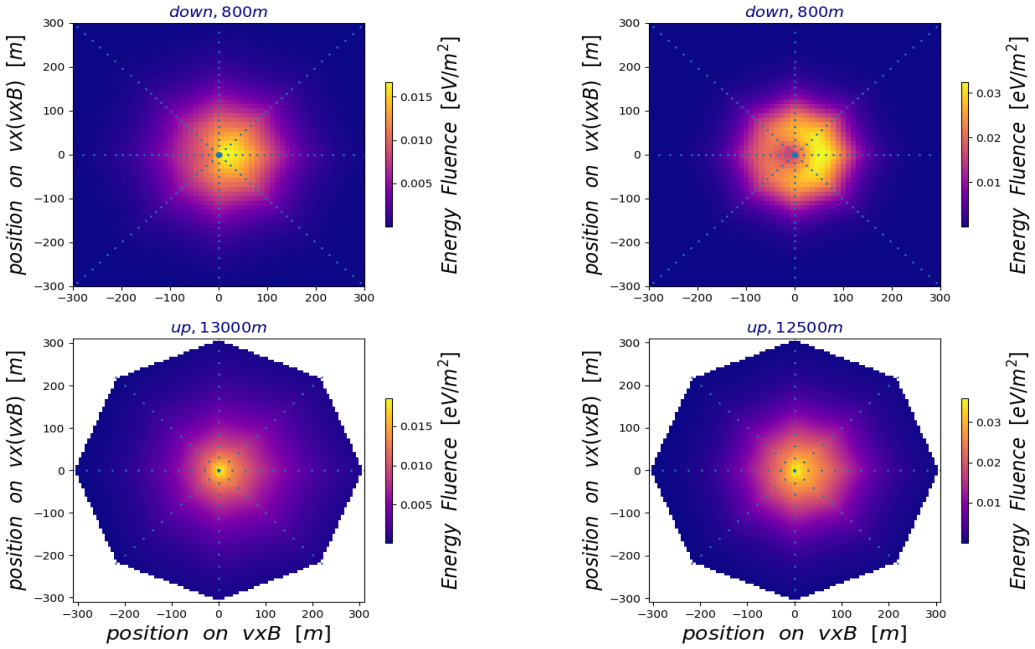

Figure 4: Distribution of the energy fluence in the 30-80 MHz band (left) and the 50-200MHz band (right) of a downward-going iron air shower with zenith angle $\theta = 0°$ with antennas at an altitude of 1 m a.s.l. (top row) and an upward-going iron air shower with zenith angle $\theta = 180°$ at an antenna altitudes of 13,000 or 12,500 m a.s.l. (lower row).

30-80 MHz				50-200 MHz			
Altitude	E_{dep} [eV]	Altitude	E_{dep} [eV]	Altitude	E_{dep} [eV]	Altitude	E_{dep} [eV]
[m]	proton	[m]	iron	[m]	proton	[m]	iron
1	$1.176 \cdot 10^3$	800	$7.970 \cdot 10^2$	1	$2.238 \cdot 10^3$	800	$1.449 \cdot 10^3$
15000	$1.215 \cdot 10^3$	12000	$7.834 \cdot 10^2$	15000	$2.420 \cdot 10^3$	12000	$1.513 \cdot 10^3$
15500	$1.225 \cdot 10^3$	12500	$7.859 \cdot 10^2$	15500	$2.452 \cdot 10^3$	12500	$1.526 \cdot 10^3$
16000	$1.228 \cdot 10^3$	13000	$7.846 \cdot 10^2$	16000	$2.470 \cdot 10^3$	13000	$1.537 \cdot 10^3$

Table 1: Radiation energy deposited at the radio antenna grids at different altitudes by proton and iron air showers. Altitude = 1 (800) m corresponds to the downward-going air showers and altitudes from 15,000 (12,000) to 16,000 (13,000) m correspond to the upward-going air showers.

5. SNR estimation on the basis of CoREAS

We use the method to predict expected SNR values described in [18] to investigate detectability of air showers for GRAND. A hexagonal layout with 301 antennas is used for this test. The radius reaches up to 7000 m on the edge. The SNR analysis is first done for each antenna for cosmic rays with primary energies from 10^{16} to 10^{17} eV. Here $SNR = S^2/N^2$ with S the maximum of a Hilbert envelope in the signal window and N the RMS noise in [50, 200] MHz.The other parameters are the same as in the previous sections. As shown in Fig. 5, three different zenith angles ($\theta = 65°$, 74°, 87°) are investigated. The results show that it will be difficult to detect a signal at 10^{16} eV,

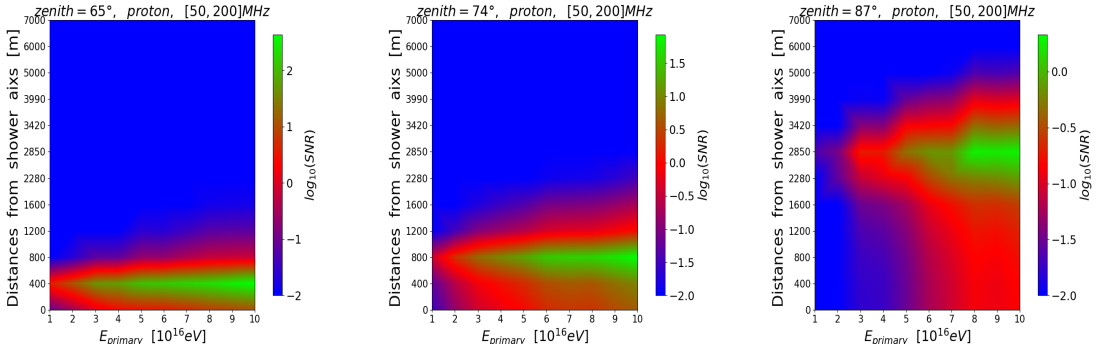

Figure 5: SNR calculated for air showers detected in the 50-200 MHz band in the presence of Galactic background. Showers were induced by protons for three zenith angles: $\theta = 65°$ (left), 74° (middle), 87° (right).

especially for larger zenith angles. However, with antennas near the Cherenkov ring, for example at 400 m axis distance for $\theta = 65°$, it seems possible to detect signals above the Galactic background. If the primary energy is below 10^{16} eV, detection will be almost impossible.

6. Conclusions

In this work, atmospheric models were analyzed for the planned GP300 site with the GDAS tool. We found that the site is located in a very stable atmosphere and that the refractive index is on average lower than at other radio detection sites. Using this atmospheric model, a library of down-going CoREAS-simulated air showers was created. Upward-going showers will be simulated with an adapted version of CORSIKA 7. We have developed the corresponding code and tested it both in terms of particle and radio simulation by comparing upward- and downward-going proton and iron air showers. The results validate the functionality of this new version since the longitudinal distribution of particle numbers and the predicted radiation energies agree for both geometries. An SNR analysis shows that it will be very difficult to detect air showers below 10^{16} eV with the testing layout of GP300, but it might be possible if the zenith angle is not too large.

Acknowledgments We thank A.Balagopal for sharing her code for the SNR calculation. C.Z. received funding from the Helmholtz-OCPC Postdoc-Program. The simulation work was performed on bwUniCluster 2.0. The authors gratefully acknowledge support by the state of Baden-Württemberg through bwHPC.

References

[1] Huege, Tim. Physics Reports 620 (2016): 1-52.
[2] Collaboration, G. R. A. N. D., Alvarez-Muniz, J., Batista, R. A., Evans, N. R., Karovska, M., Bond, H. E., ... & Solomon, A. R. (2018). Preprint at ArXiv https://arxiv. org/abs/1810.09994.
[3] Gorham, P. W., et al. Physical review letters 121.16 (2018): 161102.
[4] Huege, Tim. EPJ Web of Conferences. Vol. 210. EDP Sciences, 2019.
[5] T. Huege, M. Ludwig and C.W. James, AIP Conf. Proc. 1535 (2012) 128, arxiv:1301.2132
[6] Huege, Tim, and Clancy W. James. arXiv preprint arXiv:1307.7566 (2013).

[7] T. Antoni et al. (KASCADE Collaboration). Nuclear Instruments and Methods A, 513:490, 2003
[8] Huege, Tim, et al. Nuclear Instruments and Methods in Physics Research Section A: Accelerators, Spectrometers, Detectors and Associated Equipment 662 (2012): S72-S79.
[9] Schellart, P., et al. Astronomy & Astrophysics 560 (2013): A98.
[10] Huege, Tim, and Christoph B. Welling. EPJ Web of Conferences. Vol. 216. EDP Sciences, 2019.
[11] D. Heck, J. Knapp, J. N. Capdevielle, G. Schatz, and T. Thouw, FZKA Report 6019 (1998)
[12] Cao, Zhen, et al. Nature (2021): 1-4.
[13] National oceanic and atmospheric administration, global data assimilation system: www.ncdc.noaa.gov/data-access/model-data/model-datasets/global-data-assimilation-system-gdas
[14] Mitra, P., et al. Astroparticle Physics 123 (2020): 102470.
[15] Abreu, Pedro, et al. Astroparticle Physics 35.9 (2012): 591-607.
[16] Gorham, P. W., et al. Physical review letters 117.7 (2016): 071101.
[17] Romero-Wolf, A., et al. Physical Review D 99.6 (2019): 063011.
[18] Balagopal V., A., Haungs, A., Huege, T. et al. Eur. Phys. J. C 78, 111 (2018).

Full Authors List: GRAND Collaboration

Jaime Álvarez-Muñiz[1], Rafael Alves Batista[2], Aurélien Benoit-Lévy[3], Julien Bolmont[4], Henk Brans[2], Mauricio Bustamante[5], Didier Charrier[6], LingMei Cheng[7], Simon Chiche[8], Zigao Dai[9], Rogerio M. de Almeida[11], Valentin Decoene[12], Peter B. Denton[13], Beatriz de Errico[14], Sijbrand De Jong[2,15], João R. T. de Mello Neto[14], Krijn D. De Vries[16], Kaikai Duan[21], Ran Duan[7], Ralph Engel[17,18], Yizhong Fan[21], Ke Fang[22], QuanBu Gou[23], Junhua Gu[7], Claire Guépin[19,20], Jianhua Guo[21], Yiqing Guo[23], Rene Habraken[2,15], Andreas Haungs[17], Haoning He[21], Eric Hivon[8], Hongbo Hu[23], Xiaoyuan Huang[21], Yan Huang[7], Tim Huege[17,10], Marcelo Ismerio Oliveira[14], Ramesh Koirala[25,26], Kumiko Kotera[8,27], Wen Jiang[24], Bruno L. Lago[28], Sandra Le Coz[4], Jean-Philippe Lenain[4], Bo Liu[24], Cheng Liu[23], Ruoyu Liu[25,26], Wei Liu[23], Pengxiong Ma[21], Olivier Martineau-Huynh[4,7,8], Miguel Mostafá[29,12], Fabrice Mottez[30], Jean Mouette[8], Kohta Murase[29,12], Valentin Niess[31], Foteini Oikonomou[32], Ziwei Ou[33], Tanguy Pierog[17], Lech Wiktor Piotrowski[34], Simon Prunet[35], Xiangli Qian[36], Inge van Rens[2], Valentina Richard Romei[8], Markus Roth[17], Fabian Schüssler[37], Dániel Szálas-Motesiczky[2], Jikke Tacken[2], Anne Timmermans[2,16], Charles Timmermans[2,15], Matías Tueros[38,8], Rongjuan Wang[24], Shen Wang[21], Xiangyu Wang[25,26], Xu Wang[39], Clara Watanabe[14], Daming Wei[21], Feng Wei[24], Thei Wijnen[2], Xiangping Wu[7,40], Xuefeng Wu[41], Xin Xu[24], Xing Xu[21], Lili Yang[33], Xuan Yang[21], Qiang Yuan[21], Philippe Zarka[42], Houdun Zeng[21], Bing Theodore Zhang[12], Chao Zhang[17,43,44], Jianli Zhang[7], Kewen Zhang[4], Pengfei Zhang[24], Songbo Zhang[41], Yi Zhang[21,23], Hao Zhou[45]

[1] Departamento de Física de Partículas & Instituto Galego de Física de Altas Enerxías, Universidad de Santiago de Compostela, 15782 Santiago de Compostela, Spain
[2] Institute for Mathematics, Astrophysics and Particle Physics (IMAPP), Radboud Universiteit, Nijmegen, Netherlands
[3] Université Paris-Saclay, CEA, List, F-91120, Palaiseau, France
[4] Sorbonne Université, Université Paris Diderot, Sorbonne Paris Cité, CNRS, Laboratoire de Physique Nucléaire et de Hautes Energies (LPNHE), 4 place Jussieu, F-75252, Paris Cedex 5, France
[5] Niels Bohr International Academy, Niels Bohr Institute, 2100 Copenhagen, Denmark
[6] SUBATECH, Institut Mines-Telecom Atlantique – CNRS/IN2P3 – Université de Nantes, Nantes, France

[7] National Astronomical Observatories, Chinese Academy of Sciences, Beijing 100101, China
[8] Sorbonne Université, CNRS, UMR 7095, Institut d'Astrophysique de Paris, 98 bis bd Arago, 75014 Paris, France
[9] University of Science and Technology of China, 230026 Hefei, Anhui, China
[10] Astrophysical Institute, Vrije Universiteit Brussel, Pleinlaan 2, 1050 Brussel, Belgium
[11] Universidade Federal Fluminense, EEIMVR, Volta Redonda, RJ, Brazil
[12] Department of Physics, Department of Astronomy & Astrophysics, Pennsylvania State University, University Park, PA 16802, USA
[13] High Energy Theory Group, Physics Department,Brookhaven National Laboratory, Upton, NY 11973, USA
[14] Universidade Federal do Rio de Janeiro (UFRJ), Instituto de Física, Brazil
[15] Nationaal Instituut voor Kernfysica en Hoge Energie Fysica (Nikhef), Netherlands
[16] IIHE/ELEM, Vrije Universiteit Brussel, Pleinlaan 2, 1050 Brussels, Belgium
[17] Institute for Astroparticle Physics, Karlsruhe Institute of Technology (KIT), D-76021 Karlsruhe, Germany
[18] Institute of Experimental Particle Physics (ETP), Karlsruhe Institute of Technology (KIT), D-76021 Karlsruhe, Germany
[19] Department of Astronomy, University of Maryland, College Park, MD 20742-2421, USA
[20] Joint Space-Science Institute, College Park, MD 20742-2421, USA
[21] Key Laboratory of Dark Matter and Space Astronomy, Purple Mountain Observatory, Chinese Academy of Sciences,210023 Nanjing, Jiangsu, China
[22] Wisconsin IceCube Particle Astrophysics Center (WIPAC) and Dept. of Physics, University of Wisconsin-Madison, Madison, WI 53703, USA
[23] Institute of High Energy Physics, Chinese Academy of Sciences, 19B YuquanLu, Beijing 100049, China
[24] Key Laboratory of Antennas and Microwave Technology, Xidian University, Xi'an 710071, China
[25] School of Astronomy and Space Science, Xianlin Road 163, Nanjing University, Nanjing 210023, China
[26] Key laboratory of Modern Astronomy and Astrophysics (Nanjing University), Ministry of Education, Nanjing 210023, People's Republic of China
[27] Vrije Universiteit Brussel (VUB), Dienst ELEM, Pleinlaan 2, B-1050, Brussels, Belgium
[28] Centro Federal de Educação Tecnológica Celso Suckow da Fonseca, Nova Friburgo, Brazil
[29] Center for Multimessenger Astrophysics, Pennsylvania State University, University Park, PA 16802, USA
[30] LUTH, Obs. de Paris, CNRS, Université Paris Diderot, PSL Research University, 5 place Jules Janssen, 92190 Meudon, France
[31] Université Clermont Auvergne, CNRS/IN2P3, LPC, F-63000 Clermont-Ferrand, France.
[32] Institutt for fysikk, NTNU, Trondheim, Norway
[33] School of Physics and Astronomy, Sun Yat-sen University, Zhuhai 519082, China
[34] Faculty of Physics, University of Warsaw, Pasteura 5, 02-093 Warsaw, Poland
[35] Laboratoire Lagrange, Université Côte d'Azur, Observatoire de la Côte d'Azur, CNRS, Parc Valrose, 06104 Nice Cedex 2, France
[36] Department of Mechanical and Electrical Engineering, Shandong Management University, Jinan 250357, China
[37] IRFU, CEA, Université Paris-Saclay, F-91191 Gif-sur-Yvette, France
[38] Instituto de Física La Plata, CONICET, Boulevard 120 y 63 (1900), La Plata, Argentina
[39] Dpt. of Mechanical and Electrical Engineering, Shandong Management University, Jinan 50357,China.
[40] Shanghai Astronomical Observatory, Chinese Academy of Sciences, 80 Nandan Road, Shanghai 200030, China
[41] Purple Mountain Observatory, Chinese Academy of Sciences, Nanjing 210023, China
[42] LESIA, Observatoire de Paris, CNRS, PSL/SU/UPD/SPC, Place J. Janssen, 92195 Meudon, France
[43] Kavli Institute for Astronomy and Astrophysics, Peking University, Beijing 100871, China
[44] Department of Astronomy, School of Physics, Peking University, Beijing 100871, China
[45] Tsung-Dao Lee Institute & School of Physics and Astronomy, Shanghai Jiao Tong University, 200240 Shanghai,China

PoS(ICRC2021)248